Nat Hazards (2016) 84:2299–2319
DOI 10.1007/s11069-016-2553-0

ORIGINAL PAPER

Projection of precipitation extremes for eight global warming targets by 17 CMIP5 models

Xiaojun Guo[1,2] · Jianbin Huang[1,2] · Yong Luo[1,2] · Zongci Zhao[1,2] · Ying Xu[3]

Received: 24 May 2016 / Accepted: 22 August 2016 / Published online: 30 August 2016

Abstract Based on the historical and future outputs of 17 coupled model intercomparison project phase 5 (CMIP5) models, simulation of the precipitation extremes in China was evaluated under baseline climate condition compared to a gridded daily observation dataset CN05.1. The variations in precipitation extremes for eight global warming targets were also projected. The 17 individual models and the multi-model ensemble accurately reproduced the spatial distribution of precipitation extremes, although they were limited in their ability to capture the temporal characteristics. A notable dry bias existed in Southeast China, while a wet bias was present in North and Northwest China. The precipitation extremes in China were projected to be more frequent and more intense as global temperature rise reached the 1.5, 2.0, 2.5, 3.0, 3.5, 4.0, 4.5, and 5.0 °C warming targets. The projected percentage changes in the annual number of days with precipitation >50 mm (R50) and total precipitation during days in which the daily precipitation exceeds the 99th percentile (R99p) are projected to increase by 25.81 and 69.14 % relative to the baseline climate for a 1.5 °C warming target, and by 95.52 and 162.00 % for a 4.0 °C warming target, respectively. As the global mean temperature rise increased from 1.5 to 5 °C, the subregions considerably affected by the East Asian summer monsoon (e.g., Southwest China, South China, and the Yangtze-Huai River Valley) were projected to experience a more dramatic increase in extreme precipitation events, in both number of days and intensity, while North and Northwest China were projected to suffer from relatively slight increases. The model uncertainties in the projected precipitation extremes in China by 17 CMIP5 models increase as global temperature rise increases.

✉ Yong Luo
Yongluo@mail.tsinghua.edu.cn

[1] Ministry of Education Key Laboratory for Earth System Modeling, and Center for Earth System Science, Tsinghua University, Beijing 100080, China

[2] Joint Center for Global Change Studies (JCGCS), Beijing 100875, China

[3] National Climate Center, China Meteorological Administration, Beijing 100081, China

Keywords Precipitation extremes · Eight global warming targets · China · CMIP5 models · RCP8.5 scenario

1 Introduction

Global-scale warming has been determined to dominate climate change across the globe over the past century (IPCC 2013). Globally averaged combined land and ocean surface temperature data have indicated a warming trend of 0.85 (0.65–1.06) °C/decade from 1880 to 2012. In the Northern Hemisphere, it is likely that the period 1983–2012 was the warmest 30-year period in the last 1400 years (IPCC 2013).

In recent decades, a large number of climate extremes (e.g., heat waves, drought, extreme precipitation events) have been observed across the globe in conjunction with global warming (WMO 2010). Changes in temperature yield variations in atmospheric moisture, precipitation, and atmospheric circulation (O'Gorman and Schneider 2009). Moisture-holding capacity has been shown to increase at a rate of 7 %/°C as temperature rises, which further alters the precipitation extremes (e.g., amount, frequency, and intensity) as well as the hydrological cycle (Trenberth et al. 2003; Haerter and Berg 2009). The proportion of median intensity extreme precipitation events has been found to increase with the growth of global mean near-surface temperature at a rate ranging from 5.9 to 7.7 %/K (Westra et al. 2013).

In spite of the reduction in annual total precipitation, extreme precipitation events increased disproportionately over many mid-latitude regions compared to the mean change between 1951 and 2003 (IPCC 2007). Based on a high-quality dataset derived from 8326 land-based observation stations, Westra et al. (2013) found that there were statistically significant increases in annual maximum daily precipitation in almost two-thirds of stations across the globe from 1900 to 2009.

Compared to mean precipitation, the variations in precipitation extremes attract much more attention, especially extreme heavy precipitation events, as they and the subsequent floods they produce often adversely impact human life and society (Aguilar et al. 2009). In the last decade, numerous heavy precipitation events and floods have been observed around the world (WMO 2010; Coumou and Rahmstorf 2012). Precipitation extremes were also frequently observed across China and have had disastrous impacts in recent decades. In 1998, the entire Yangtze River area suffered from the largest flood event since 1954 due to unusually high precipitation (670 mm) caused by a strong El Niño event between June and August (Yin and Li 2001). Approximately 233 million people were affected, and approximately 4,970,000 houses were razed (Zong and Chen 2000). From July 21 to 22, 2012, Beijing, the capital of China, suffered from the largest flood event since 1954. Approximately 86 % of the city received over 100 mm of precipitation. The heaviest rain was observed in Fangshan District where precipitation reached approximately 460 mm (Wang et al. 2013). This severe flood affected more than 1.6 million people and led to 79 natural hazard (e.g., lightning, landslides, drowning)-related deaths. In addition, 63 main roads flooded, and almost 20,000 automobiles were immersed and bridges were broken (Wang et al. 2013; Zhang et al. 2013b). This flooding resulted in enormous, direct economic losses for China, losses that were estimated at around £12,815 million for the 1998 Yangtze River flood and over US $1.86 billion caused by the 2012 Beijing flood (Zong and Chen 2000; Zhang et al. 2013b).

In general, the changes in precipitation extremes coincide with a wetter climate (IPCC 2013). It is likely that both the frequency and amount of heavy rainfall will increase over most regions of the globe in the twenty-first century (Field et al. 2012). Given China's vast territory and complex topography, climate extremes across the country vary with spatiotemporal scale (Gao et al. 2008). Regional precipitation variability is one of the major climatic characteristics associated with China (Qian and Lin 2005). Because it is strongly affected by the East Asian Monsoon System, China is vulnerable to frequent climatic hazards, especially floods caused by heavy rainfall. Thus, in this study, we will investigate the variations in precipitation extremes over different subregions across China, especially in the East Asian summer monsoon regions. Using 7 CMIP3 models, Jiang et al. (2012) projected that precipitation extremes would be more frequent and intense across China by the end of twenty-first century, with significant increases found primarily in the middle and lower reaches of the Yangtze River, the Southeast coastal region, the west part of Northwest China, and the Tibetan Plateau. In their study using 24 CMIP5 models, Zhou et al. (2014) found that precipitation extremes evidenced disproportionately larger percentage increases compared to mean precipitation.

With the growing attention on climate change's impacts on ecosystems, system vulnerabilities, and overall threats, restricting the global mean temperature rise to a safer level has been a hot topic for policymakers from different nations. A 2 °C warming relative to pre-industrial times was supported and accepted by many countries in a Conference of the Parties (UNFCCC 2009; UNFCCC 2013) and has been commonly regarded as the most essential target in climate policy negotiations (Tschackert 2015). However, there is still considerable debate about whether temperature rise should be restricted below 1.5 °C or 2 °C. The demand for a 1.5 °C maximum warming target has primarily been supported by the less developed and more vulnerable countries, as they would face more considerable threats if temperature rise exceeds 2 °C (Kanitkar 2015). At the 21st Conference of the Parties (COP21) held in Paris in December 2015, the goal to limit the warming target below 1.5 °C was explicitly identified and included in the final accepted draft of the Paris agreement (Kanitkar 2015). According to climate model projection results, the global mean temperature rise is expected to reach the 4, 4.5, and 5 °C warming targets by the end of twenty-first century (Zhang et al. 2013a; Guo et al. 2016). Thus, it is imperative that researchers investigate the variation in precipitation extremes across China using these higher warming targets. Guo et al. (2016) have shown that heat waves over China will be more frequent, longer lasting, and more intense as the global warming target increases from 1.5 to 5 °C. Future changes in precipitation events are more complicated than changes in temperature (Luo et al. 2005). Using a high-resolution regional climate model RegCM3, Lang and Sui (2013) found that the number of days where daily precipitation was $\geq$10 mm/day and the maximum 5-day total precipitation for China would increase by 0.4 days and 5.1 mm for a 2 °C warming target with respect to the baseline period (1986–2005). In the present study, 17 CMIP5 models are tested to explore the changes in precipitation extremes across China to guarantee the confidence and reliability of the projection results to a certain degree.

The purpose of this study is to explore the characteristics of changes in extreme heavy precipitation events for eight global warming targets (1.5, 2.0, 2.5, 3.0, 3.5, 4.0, 4.5, and 5.0 °C), which will inform policymakers' understanding of the potential impacts of climate change, allow for the formation of appropriate adaptation strategies, and support an agreement related to the international negotiations on climate change. Data and methods are provided in Sect. 2. An evaluation of the precipitation extremes based on 17 CMIP5 climate models is in Sect. 3. In Sect. 4, the projected change in precipitation extremes

across China and six subregions is displayed for eight warming targets using these models, and an uncertainty analysis is performed. A discussion and conclusions are provided in Sect. 5.

2 Data and methods

2.1 Model and observation dataset

The CMIP5 global climate models (GCMs) are very beneficial tools for analyzing climate change. To better project precipitation extremes, 17 state-of-the-art CMIP5 GCMs are adopted in this study. Each model is the most widely used and representative model within its group. These models' details are provided in Table 1.

The ability of these CMIP5 models to simulate precipitation extremes is assessed using a daily gridded observation dataset CN05.1 (0.5° × 0.5°), which was established by the China Meteorological Administration. This dataset was interpolated from 2416 observation stations and covers the period 1961–2013 (Wu and Gao 2013). It has been widely used in many studies of precipitation extremes across China (Gao et al. 2013; Ji and Kang 2015).

2.2 Analyzed time period and calculation method

2.2.1 Selection of the analyzed time period

The primary rainy season in Eastern China corresponds with the progress of the East Asian summer monsoon (EASM), which is the most distinctive climatic feature in this region (Zhai et al. 2005). The EASM generally develops from May to September and accounts for

Table 1 Details of the 17 CMIP5 global climate models used in this research

Model	Institute/country	Resolution	Historical period	Future period
ACCESS1-0	CSIRO-BOM/Australia	192 × 145	1850–2005	2006–2100
BCC-CSM1-1	BCC/China	128 × 64	1850–2012	2006–2100
BNU-ESM	GCESS/China	128 × 64	1850–2005	2006–2100
CanESM2	CCCMA/Canada	128 × 64	1850–2005	2006–2100
CCSM4	NCAR/America	288 × 192	1850–2005	2006–2100
CMCC-CM	CMCC/Italy	480 × 240	1850–2005	2006–2100
CNRM-CM5	CNRM-CERFACS/France	256 × 128	1850–2005	2006–2100
CSIRO-Mk3.6.0	CSIRO-QCCCE/Australia	192 × 96	1850–2005	2006–2100
FGOALS-s2	LASG-CESS/China	128 × 60	1850–2005	2006–2100
GFDL-ESM2G	NOAA GFDL/America	144 × 90	1861–2005	2006–2100
HadGEM2-ES	MOHC/England	192 × 145	1860–2005	2006–2100
IPSL-CM5A-LR	IPSL/France	96 × 96	1850–2005	2006–2100
MIROC-ESM-CHEM	MIROC/Japan	128 × 64	1850–2005	2006–2100
MIROC5	MIROC/Japan	256 × 128	1850–2005	2006–2100
MPI-ESM-MR	MPI-M/German	192 × 96	1850–2005	2006–2100
MRI-CGCM3	MRI/Japan	320 × 160	1850–2005	2006–2100
NorESM1-M	NCC/Norway	144 × 96	1850–2005	2006–2100

60–85 % of the total annual rainfall over most regions of China (Gao et al. 2008). Thus, precipitation extremes are analyzed during the monsoon season (May–September) in this study. The time period from 1971 to 2000 (total 30 years) has been adopted as the baseline period, and the time period from 1861 to 1880 (total 20 years) has been selected to represent the pre-industrial timeframe (Meehl et al. 2012). The reasons for choosing this pre-industrial period are explicitly elucidated in Guo et al. (2016).

2.2.2 Calculation method

Based on previous research by Jiang and Fu (2012), the year at which the difference between the global surface air temperature (SAT) series from 2006 to 2099 and the globally averaged SAT of the pre-industrial time period reaches a specific warming target is regarded as the median year for that target. The change in the extreme precipitation index is calculated by subtracting the 9-year average of this index by that of the baseline climate. The 9 years used for this average include the median year for which global mean surface temperature crosses a given warming target, as well as the 4 years preceding and following the median year. The multi-model ensemble (MME) was calculated using equal weights.

2.3 Definition of extreme precipitation indices

A universally valid definition of extreme precipitation is difficult to provide because of the diversity of climates across the globe (IPCC 2013). In general, most studies of global precipitation extremes adopt the indices established by the Expert Team on Climate Change Detection and Indices (ETCCDI). Heavy precipitation days (R10) and very heavy precipitation days (R20) are two common indices used to demonstrate the frequency of precipitation extremes (IPCC 2007, 2013). In China, precipitation is divided into the following five categories: trace rain (0.1–1.0 mm/day), light rain (1.0–10 mm/day), medium rain (10–25 mm/day), large rain (25–50 mm/day), and heavy rain (>50 mm/day); these categories have been widely used in previous research across the country (Sun et al. 2007; Huang et al. 2013). In particular, heavy and severe rainstorms in China are traditionally defined as events with daily precipitation values greater than 25, 50, and 100 mm (Domroes and Peng 1988; Zhai et al. 2005). In this study, we explore the more severe precipitation extremes. Thus, the absolute thresholds of 25 mm/day and 50 mm/day are chosen to define precipitation extremes in this work. R25 and R50 are defined as the cumulative number of days during which daily precipitation exceeds the 25 mm and 50 mm, respectively (Table 2).

Furthermore, using the precipitation indices recommended by the ETCCDI, R95p and R99p, which have been widely used in many studies, have been selected to represent the intensity of these precipitation extremes (Table 2) (Klein Tank et al. 2006; You et al. 2011). By adopting a percentile threshold for this parameter, the effects caused by differences in the mean climate state of precipitation between individual models can largely be ignored.

Thus, four extreme precipitation indices have been adopted in this study to investigate changes in the frequency and intensity of heavy rainfall in China. Detailed definitions of these indices are described in Table 2.

Table 2 Definitions of extreme precipitation indices used in this study

Extreme precipitation indices	Definition (unit)
R25	The cumulative number of precipitation days during which daily precipitation exceeds 25 mm per year (days)
R50	The cumulative number of precipitation days during which daily precipitation exceeds 50 mm per year (days)
R95p	The total amount of precipitation during days in which daily precipitation exceeds the 95th percentile of the reference period 1971–2000 per year (mm)
R99p	The total amount of precipitation during days in which daily precipitation exceeds the 99th percentile of the reference period 1971–2000 per year (mm)

2.4 Division of six subregions in China

Climate extremes are largely affected by distinct topography (Zhai et al. 2005; Qian and Lin 2005). Due to the effects of the East Asian monsoon system and varied topography in China, the annual amounts of precipitation vary nationally from less than 25 mm in the northwest to more than 2000 mm in the southeast (Zhai et al. 2005). To investigate the characteristics of regional changes in precipitation extremes for eight warming targets, the country has been divided into six subregions based on geographical conditions and climatic features (Fig. 1). Detailed information regarding these six subregions is provided in Table 3.

3 Evaluation of precipitation extremes in China simulated by 17 CMIP5 models

3.1 Evaluation of model-simulated temporal variability of precipitation extremes

Compared to temperature extremes, precipitation extremes are more complex climate events. It is much more difficult for climate models to simulate the features of precipitation

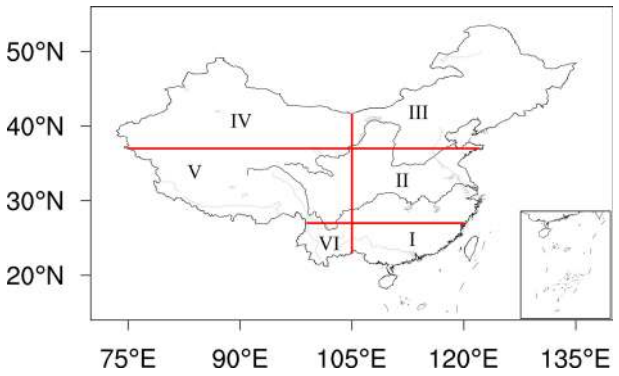

Fig. 1 Map of China's six geographical subregions

Table 3 Details of six subregions in China

Subregion name	Subregion number	Latitude	Longitude
South China (SC)	I	20–27°N	105–120°E
Yangtze-Huai River Valley (YH)	II	27–37°N	105–120°E
Northeast China (NEC)	III	37–55°N	105–135°E
Northwest China (NWC)	IV	37–47°N	75–105°E
Qinghai-Tibet region (QT)	V	27–37°N	75–105°E
Southwest China (SWC)	VI	20–27°N	98–105°E

extremes (Jiang et al. 2012). As shown in Table 4, the observed linear trends for R25, R50, R95p, and R99p in China from 1961 to 2005 are 0.06 days/10a, 0.05 days/10a, 2.50 mm/10a, and 0.08 mm/10a, respectively, which indicates that heavy precipitation extremes have slightly increased across China as a whole. However, the linear trends in these four indices as simulated by the model ensemble are 0.02 days/10a, 0.01 days/10a, 1.28 mm/10a, and −0.20 mm/10a, respectively. Although the MME generally captures the positive trends in extreme heavy precipitation events, the values of the simulated trends are significantly lower than those of the observed trends. In particular, the linear trends as simulated by individual models vary greatly. In total, 8, 7, 10, and 6 out of 17 models simulated positive trends for the R25, R50, R95p, and R99p indices, respectively, which are consistent with the observed positive trend.

In general, the CMIP5 models are limited in their ability to simulate the temporal variability of extreme heavy precipitation events during 1961–2005, although half of these models are able to simulate the observed positive trend.

3.2 Evaluation of model-simulated spatial features of precipitation extremes

The ability to simulate the spatial features of precipitation extremes varies from model to model. As shown in Fig. 2, 11 models overestimate the R25 while 12 models underestimate the R50. Eleven and 10 models simulate higher R95p and R99p, respectively, compared with the observation data. The relative bias for R25, R50, R95p, and R99p between the MME and the observation data is 16.9, −10.3, 8.4, and 4.3 %, respectively. The model ensemble underestimates the total number of extreme precipitation days during which daily precipitation exceeds 50 mm while other indices are overestimated. This

Table 4 Observed and simulated linear trends in four extreme precipitation indices for the 17 CMIP5 models and the MME from 1961 to 2005

Linear trend	R25 (days/10a)	R50 (days/10a)	R95p (mm/10a)	R99p (mm/10a)
Ensemble (ranges of individual model simulations)	0.02 (−0.27 to 0.21)	0.01 (−0.08 to 0.11)	1.28 (−4.38 to 8.05)	−0.20 (−2.47 to 3.36)
Observed value	0.06	0.05	2.50	0.08

The values in brackets indicate the ranges of simulated linear trends by the 17 individual models

suggests that the CMIP5 models and the MME are still unable to adequately capture the more severe heavy precipitation events.

The spatial correlation coefficients (SCCs) between individual models and the observed data for the four extreme precipitation indices range from 0.06 to 0.87, 0.03 to 0.75, 0.47 to 0.85, and 0.48 to 0.84, respectively. The SCCs for the model ensemble are 0.64, 0.58, 0.81, and 0.81, respectively. The SCCs for extreme precipitation days between most of the models and the observed data can exceed 0.4, with the SCC for the MME reaching 0.48. It is noteworthy that 15 of the 17 SCCs exceeded 0.6 for both the R95p and R99p indices. In terms of the simulation capacity of each model, of the 17 GCMs, HadGEM2-ES is best able to simulate the spatial features of these four indices with a relative bias (SCC) of approximately 4.15 % (0.87), −0.84 % (0.75), 8.37 % (0.84), and 1.67 % (0.84) for R25, R50, R95p, and R99p, respectively.

In terms of the spatial distribution of precipitation extremes, the East Asia monsoon rainfall was at a maximum in Southeast China and significantly decreased toward North and Northwest China (Fig. 3), which is consistent with the results presented by Gao et al. (2008). Compared to the observation dataset, the spatial distribution of precipitation extremes simulated by the MME indicates a reduction in the spatial contrast over Southern and Eastern China. The largest observed precipitation center is located in Guangdong and Fujian provinces, the middle and lower reaches of the Yangtze River, the Southeastern Tibetan Plateau, and the Sichuan basin, which is consistent with previous results (Zhai

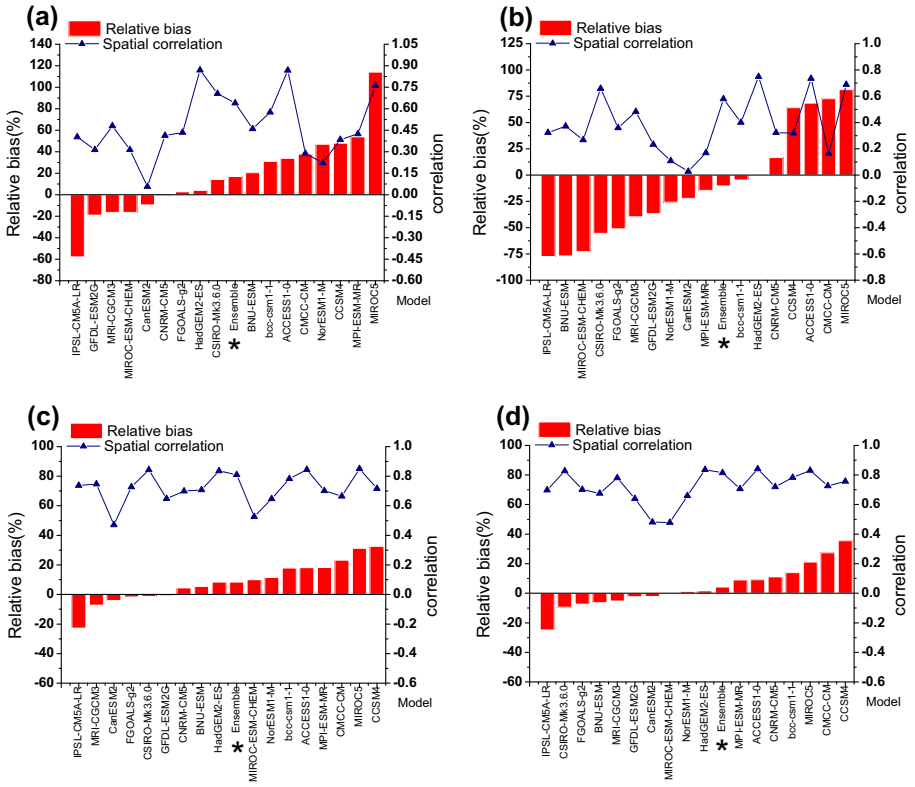

Fig. 2 Relative bias ((model-observation)/observation × 100) (unit: %) (*red bars*) and spatial correlation coefficients (*blue lines*) between model simulations and observations during the baseline period (1971–2000) for **a** R25, **b** R50, **c** R95p, and **d** R99p

et al. 2005; Gao et al. 2008; Li and Luo 2011). However, the ranges and magnitude of strong precipitation events in the middle and lower reaches of the Yangtze River are poorly represented by the MME because the spatial variations in this region are smoothed out when the results of the 17 individual models are averaged. Additionally, the total number of days during which the daily precipitation exceeds 50 mm annually is almost zero in Northwest China, which indicates that heavy precipitation events are very rare in this vast region (Zhai et al. 2005). As observed in Table 5, the nationally averaged extreme precipitation indices during the baseline period are adequately captured by the 17 individual CMIP5 models and the model ensemble.

The four extreme precipitation indices display similar spatial distribution patterns related to bias (Fig. 4). There is a significant wet bias in the rainfall-deficient regions (e.g., Western and Northern China), while there is a large dry bias in the frequent rainfall regions (e.g., the middle and lower reaches of the Yangtze River and Southeast China), which is consistent with the results provided by Jiang et al. (2015). It is noteworthy that a strong positive precipitation bias occurs along the southeastern edge of Tibetan Plateau, a finding that is consistent with a number of previous results (Gao et al. 2008; Jiang et al. 2012, 2015). The model ensemble overestimates the R25, R50, R95p, and R99p indices along the region from the southeastern edge of the Tibetan Plateau to Sichuan Province by approximately 19.6 days/year, 6.1 days/year, 390.5 mm/year, and 103.1 mm/year, while it underestimates the four indices in Guangdong Province and the middle-lower reaches of

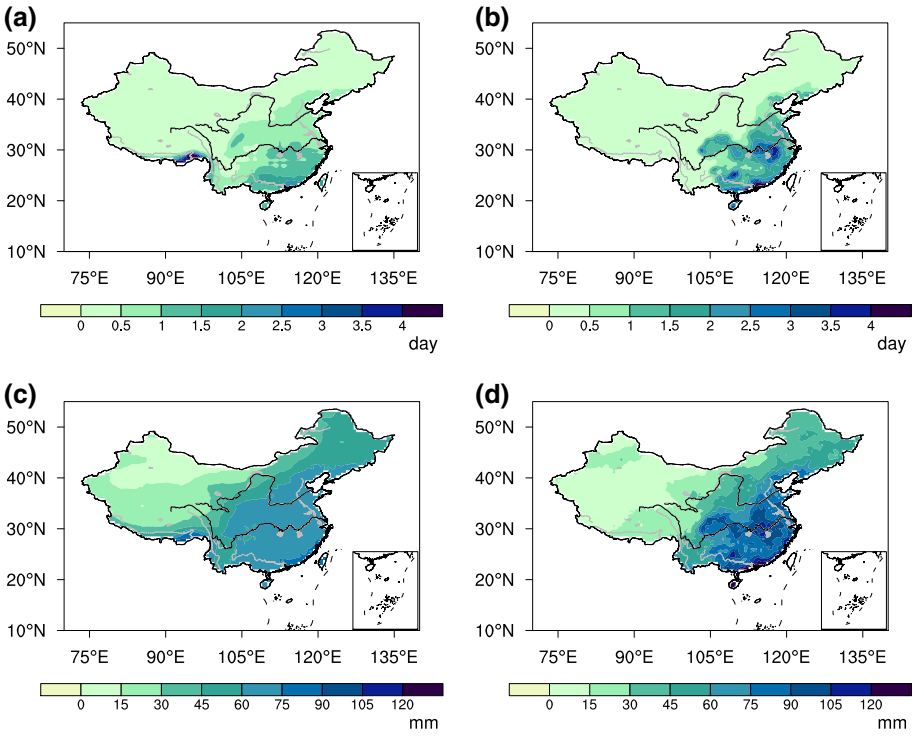

Fig. 3 Spatial distribution of extreme precipitation indices for **a** R50_MME (unit: days), **b** R50_observation (unit: days), **c** R99p_MME (unit: mm), and **d** R99p_observation (unit: mm) during the baseline period (1971–2000)

Table 5 Observed and simulated nationally averaged extreme precipitation indices for the 17 CMIP5 models and the MME from 1971 to 2000

National averaged values	R25 (days)	R50 (days)	R95p (mm)	R99p (mm)
Ensemble (ranges of individual model simulations)	3.2 (1.2–5.9)	0.4 (0.1–0.9)	154.5 (110.2–189.1)	44.1 (31.7–57.6)
Observed data	2.7	0.5	142.4	42.3

The values in brackets indicate the ranges of simulated indices for the 17 individual models

the Yangtze River by approximately 11.6 days/year, 4.8 days/year, 256.2 mm/year, and 95.4 mm/year, respectively. In general, compared to the observation data, most of the individual models and the MME tend to simulate higher frequency and amount of extreme precipitation in the arid regions, while they simulate less extreme precipitation in the regions strongly influenced by the EASM.

The above analysis indicates that the 17 individual models and the MME can accurately reproduce the spatial features of observed precipitation extremes in China, although they are limited in their ability to capture temporal features.

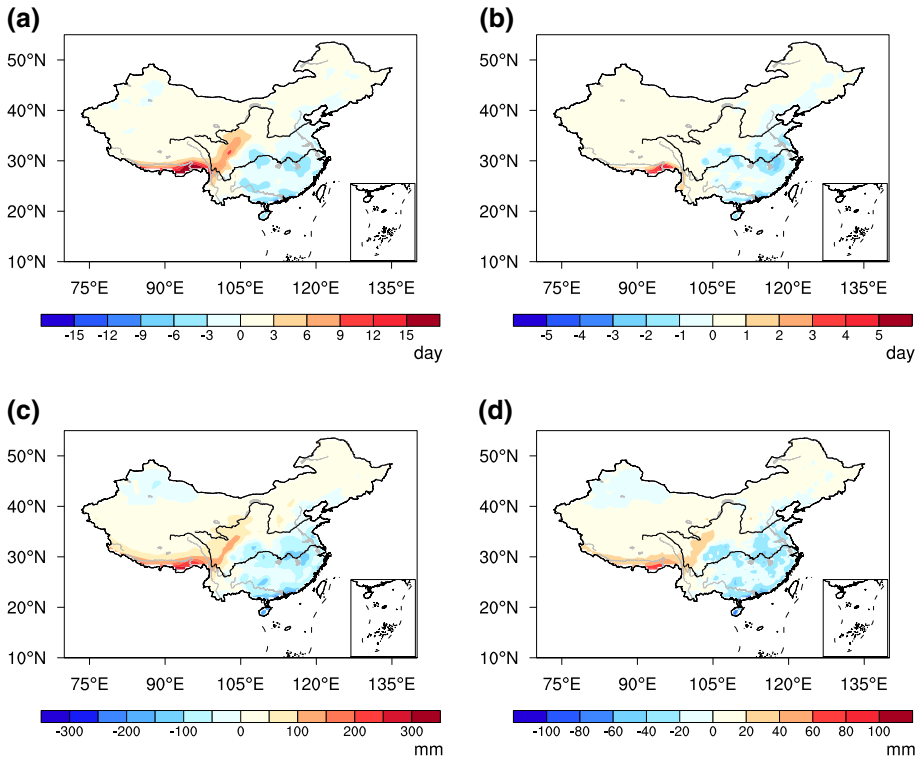

Fig. 4 Spatial distribution of bias (model ensemble simulation minus observation) for **a** R25 (unit: days), **b** R50 (unit: days), **c** R95p (unit: mm), and **d** R99p (unit: mm) during the baseline period (1971–2000)

4 Projection of precipitation extremes in China for eight global warming targets

4.1 Temporal evolution of precipitation extremes in China from 2006 to 2099

As shown in Fig. 5, the four nationally averaged extreme precipitation indices reveal increasing trends for the period 2006–2099. These linear trends for the RCP8.5 scenario are approximately 2–3 times as large as those for the RCP4.5 scenario (Fig. 5). The rate of increase for the R25 (R95p) index is approximately 3 (1.5) times as large as that for the R50 (R99p) index for the RCP8.5 scenario, which indicates that more daily precipitation will exceed the lower criterion (e.g., 25 mm, 95th percentile). By 2099, the nationally averaged R25, R50, R95p, and R99p values are projected to increase to approximately 3.9 (5.0) days, 0.7 (1.1) days, 215.0 (281.8) mm, and 95.2 (145.3) mm under the RCP4.5 (RCP8.5) scenario, respectively. Overall, these results indicate that extreme precipitation events will be more frequent and more intense than at present under two RCP scenarios, especially the RCP8.5 scenario, by the end of the twenty-first century.

4.2 Projected timings to reach eight warming targets using the 17 CMIP5 models

The median years in which the eight warming targets would be reached as determined by the 17 CMIP5 models and the MME under the RCP4.5 and RCP8.5 scenarios are provided in Fig. 6. Under the RCP8.5 scenario, as global temperature rise exceeds the warming

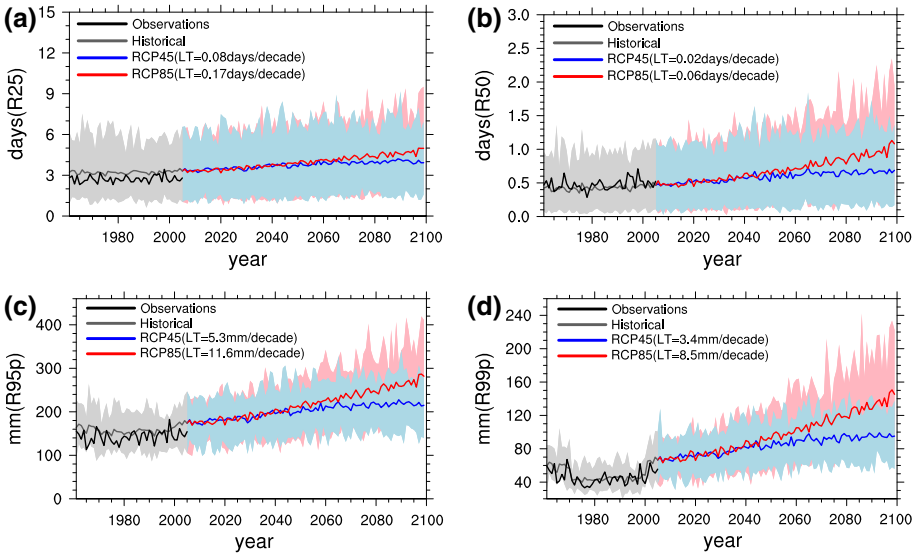

Fig. 5 Temporal evolution of **a** R25 (unit: days), **b** R50 (unit: days), **c** R95p (unit: mm), and **d** R99p (unit: mm) simulated and projected by the MME during the 1961–2099 period and from the observation data for 1961–2005. The *black line* indicates the observation results, while the *gray line* indicates the historical simulation results; the *blue line* indicates the projection results under the RCP4.5 scenario, while the *red line* indicates the projection results under the RCP8.5 scenario. The *shading* indicates the range of simulation results by 17 CMIP5 models. The *brackets* in the legend of each *figure* indicate the linear trends of the precipitation index under the RCP4.5 and RCP8.5 scenarios during the 2006–2099 period

target of 3.5 °C, the number of models able to project this rise in temperature decreases, with 13, 12, and 7 models able to project a temperature increase of 4, 4.5, and 5 °C, respectively. The specific warming target is crossed earlier for the RCP8.5 scenario than the RCP4.5 scenario. For example, the median years projected by the MME under the RCP4.5 (RCP8.5) scenario are 2027 (2024), 2047 (2038), and 2075 (2050) when global temperature rise attains 1.5, 2.0, and 2.5 °C warming targets, respectively.

Because none of these models can simulate a temperature increase above 3 °C relative to the pre-industrial period under the RCP4.5 scenario, the variation in precipitation extremes will be explored for eight warming targets under the RCP8.5 scenario to investigate these variations under higher warming targets (e.g., 3.5, 4, 4.5, and 5 °C).

4.3 Spatial distribution of precipitation extremes in China for the 2 °C global warming target

The spatial distribution of variations in precipitation extremes by the MME for the 2 °C warming target is given in Fig. 7. This distribution reveals similar spatial increase patterns for all indices. When the global temperature rise reaches 2 °C, the projected increase in nationally averaged R25, R50, R95p, and R99p indices values are approximately 0.45 (0.13–1.01) days/year, 0.17 (0.08–0.37) days/year, 42.00 (20.91–81.11) mm/year, and 38.34 (20.71–66.12) mm/year, respectively. In Eastern China, the largest increases in frequency and amount of precipitation occur in South China and the Yangtze-Huai River Valley, with increase values for the R25, R50, R95p, and R99p indices at approximately 1.5 days/year, 0.5 days/year, 70 mm/year, and 140 mm/year, respectively, relative to the baseline climate data. In Western China, the four indices measured in Southwest China and the Southeastern Tibetan Plateau show the clearest increase in precipitation, exceeding 2 days/year, 1 day/year, 200 mm/year, and 100 mm/year, with a significant strong rain band extending from the Southern to Eastern Tibetan Plateau. In some regions of Western China, particularly where rainfall occurs extremely rarely, the number of days during which daily precipitation exceeds 25 mm or even 50 mm (i.e., R25, R50) are projected to decrease.

4.4 Spatial distribution of precipitation extremes in China for eight global warming targets

The spatial distributions of the variations in the R50 and R99p indices are provided in Figs. 8 and 9. The precipitation extremes are projected to be more intense and more

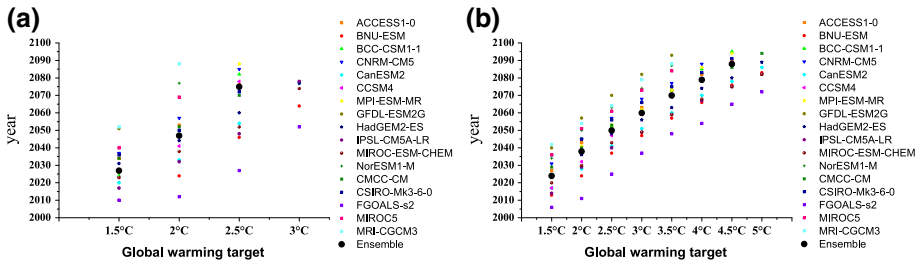

Fig. 6 Median years projected by the 17 CMIP5 models and the MME for eight global warming targets (1.5, 2.0, 2.5, 3.0, 3.5, 4.0, 4.5, and 5.0 °C) under the **a** RCP4.5 and **b** RCP8.5 scenario. Black dots indicate the MME results

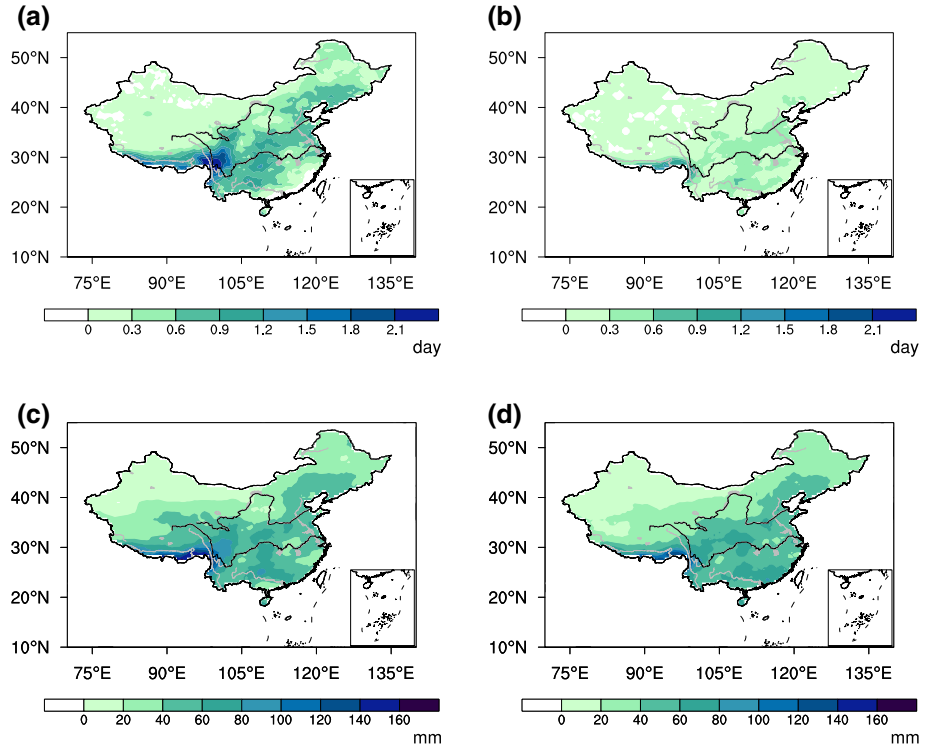

Fig. 7 Spatial distribution of variation in **a** R25 (unit: days), **b** R50 (unit: days), **c** R95p (unit: mm), and **d** R99p (unit: mm) projected by the MME for a 2 °C warming target under the RCP8.5 scenario (relative to the baseline period 1971–2000)

frequent as the global mean temperature rise reaches the 1.5, 2.0, 2.5, 3.0, 3.5, 4.0, 4.5, and 5.0 °C warming targets. In particular, those regions that are considerably affected by the EASM and have more heavy precipitation events in the baseline climate period (e.g., Southwest China, South China, and the middle and lower reaches of the Yangtze River) will suffer from even more severe precipitation extremes, in both number and intensity. Both the increase in the frequency and amount of extreme precipitation contributes to the increase in heavy rainfall in EASM-affected areas. Compared to these areas, the vast region of North and Northwest China will experience lower increases in precipitation, especially the number of days in which daily precipitation exceeds 50 mm.

In terms of the increase in value and rate of these four extreme precipitation indices shown in Tables 6 and 7, R99p will increase by 69, 87, 110, 135, 158, 162, 185, and 209 % for the 1.5, 2.0, 2.5, 3.0, 3.5, 4.0, 4.5, and 5.0 °C warming targets compared to the R99p of 44.1 mm/year in the baseline climate period, respectively, which indicates a gradually increasing trend. The number of days during which daily precipitation exceeds 50 mm (i.e., R50) are projected to exhibit increase at a greater rate than R25. For example, for the 1.5 °C warming target, the increase rates for R50 and R25 are approximately 25.81 and 8.14 %, respectively, with respect to the baseline climate. Similarly, R99p is projected to increase at a greater rate than R95p. These results indicate that heavier precipitation will be more frequent and intense as higher warming targets are crossed.

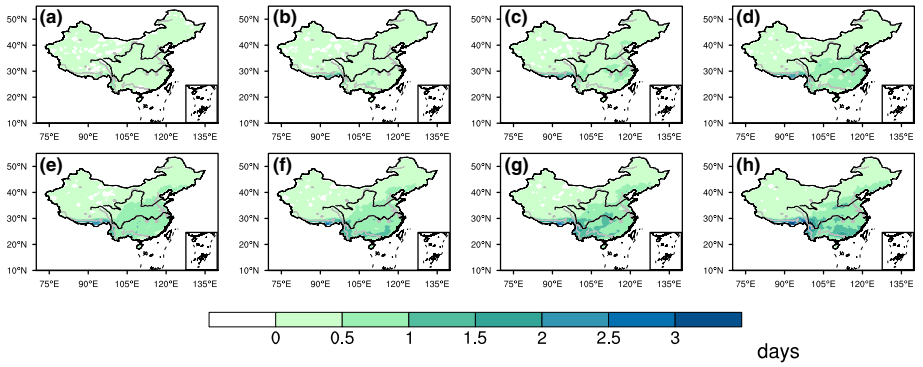

Fig. 8 Spatial distribution of variation in R50 projected by the MME for global warming targets of **a** 1.5 °C, **b** 2.0 °C, **c** 2.5 °C, **d** 3.0 °C, **e** 3.5 °C, **f** 4.0 °C, **g** 4.5 °C, and **h** 5.0 °C under the RCP8.5 scenario (relative to the baseline period 1971–2000) (unit: days)

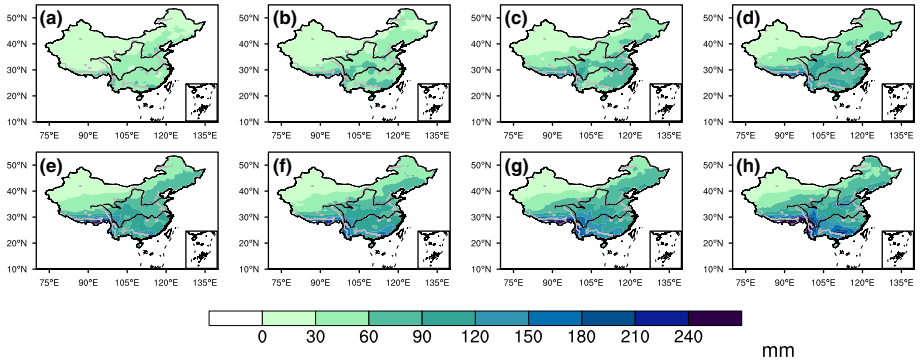

Fig. 9 Spatial distribution of variation in R99p projected by the MME for global warming targets of **a** 1.5 °C, **b** 2.0 °C, **c** 2.5 °C, **d** 3.0 °C, **e** 3.5 °C, **f** 4.0 °C, **g** 4.5 °C, and **h** 5.0 °C under the RCP8.5 scenario (relative to the baseline period 1971–2000) (unit: mm)

Table 6 Increase in value (IV) of four nationally averaged extreme precipitation indices projected by the MME for eight warming targets under the RCP8.5 scenario (relative to the baseline period 1971–2000)

IV	1.5 °C	2 °C	2.5 °C	3 °C	3.5 °C	4 °C	4.5 °C	5 °C
R25 (days/year)	0.26	0.45	0.66	0.94	1.11	1.14	1.30	1.46
R50 (days/year)	0.11	0.17	0.23	0.31	0.37	0.40	0.47	0.52
R95p (mm/year)	30.41	42.00	56.64	73.49	86.19	88.34	99.63	113.95
R99p (mm/year)	30.51	38.34	48.47	59.46	69.58	71.59	81.41	92.29

4.5 Characteristics of variations in precipitation extremes for eight global warming targets in six subregions

As the global mean temperature rise increases from 1.5 to 5 °C, the increase of R25, R50, R95p, and R99p in all six of China's subregions tends to increase (Fig. 10). Southwest China exhibits the greatest increase in frequency and intensity of precipitation extremes, while Northwest China experiences the smallest increase. For example, R99p increases by

Table 7 Rate of increase (IR) (unit: %) for four nationally averaged extreme precipitation indices projected by the MME for eight warming targets under the RCP8.5 scenario (relative to the baseline period 1971–2000)

IR (%)	1.5 °C	2 °C	2.5 °C	3 °C	3.5 °C	4 °C	4.5 °C	5 °C
R25	8.14	14.08	20.65	29.42	34.74	37.10	67.67	75.99
R50	25.81	39.89	53.97	72.74	86.82	95.52	109.41	121.05
R95p	19.69	27.19	36.67	47.57	55.80	57.23	85.31	97.57
R99p	69.14	86.89	109.85	134.75	157.69	162.00	184.52	209.18

Calculation used to determine the rate of increase in extreme precipitation indices

$$\text{Increase rate for selected target} = \frac{(\text{Mean value of selected target} - \text{mean value of baseline climate data})}{\text{mean value of baseline climate data}\,(1971-2000)} \times 100$$

54.32 (10.88) mm/year for the 1.5 °C warming target and 150.85 (21.66) mm/year for the 4 °C warming target in Southwest China (Northwest China), with respect to the baseline climate value of 60.80 (16.40) mm/year. Additionally, South China and the Yangtze-Huai River Valley will also experience relatively large increases, with the increase in R99p of each of these regions nearly double that of values in the Northeast China, where extreme precipitation is projected to increase second least.

Overall, as the global temperature rise increases from 1.5 to 5 °C, the subregions that are greatly affected by the EASM (e.g., Southwest China, South China, and the Yangtze-Huai River Valley) will suffer from more extreme precipitation events with greater intensities. In contrast, the subregions where low extreme precipitation was recorded in the baseline climate (e.g., Northwest China) will experience smaller increases in extreme precipitation.

4.6 Uncertainty analysis of the projected precipitation extremes in China for eight global warming targets

The uncertainty values related to the projected precipitation extremes are provided by box plots in Fig. 11. The uncertainty in the number of projected extreme precipitation days and amount of precipitation by the 17 CMIP5 models will increase as global temperature rise reaches the higher warming targets. For example, the projected change in R25 (R95p) in China varies from −0.11 days/year (14.83 mm/year) to up to 0.64 days/year (54.57 mm/year) for the 1.5 °C warming target while it varies from 0.33 days/year (45.44 mm/year) up to 1.73 days/year (128.73 mm/year) for the 3.5 °C warming target.

The intermodel standard deviation (STD_m) is a widely used indicator for quantifying uncertainty (Li and Zhou 2010). As observed from Fig. 12, the STD_m of changes in R95p for the 1.5 and 3.5 °C warming targets is much larger along the southeastern edge of the Tibetan Plateau, Southwest China, South China, and the Yangtze-Huai River Valley compared to the other regions. For example, the maximum STD_m of R95p in South China (Qinghai-Tibet region) increases from 96.5 (91.9) mm for the 1.5 °C warming target to 126.8 (252.3) mm for the 3.5 °C warming target, which indicates that the uncertainty along the southeastern edge of the Tibetan Plateau will increase more rapidly as the global warming target increases. Compared to those regions with a relatively smaller increase in extreme precipitation (e.g., Northwest China), the larger uncertainty in the projected extreme precipitation values will occur in those regions that experience greater increases in heavy precipitation events, which is consistent with the results provided by Xu et al. (2015).

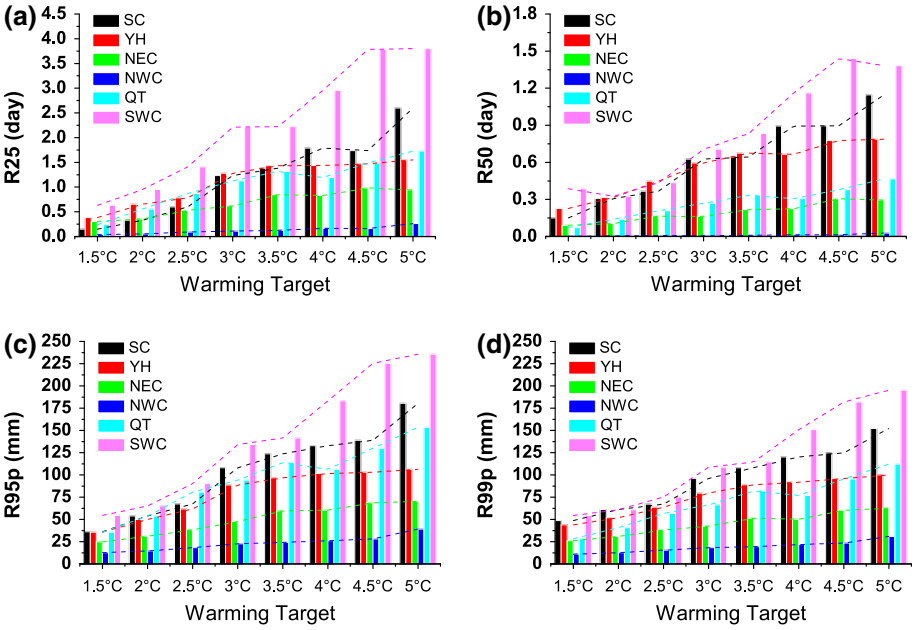

Fig. 10 Increase in value (IV) for **a** R25 (unit: days), **b** R50 (unit: days), **c** R95p (unit: mm), and **d** R99p (unit: mm) projected by the MME in six subregions for eight warming targets under the RCP8.5 scenario (relative to the baseline period 1971–2000)

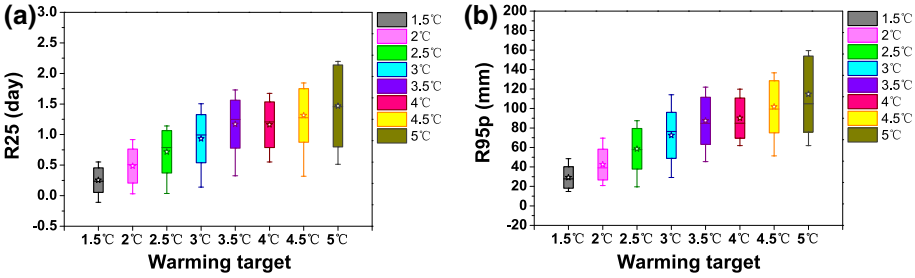

Fig. 11 Changes in extreme precipitation days R25 and amounts R95p projected by the 17 CMIP5 models and the MME for eight global warming targets under the RCP8.5 scenario relative to the baseline period (1971–2000). For each box plot, the *top* and *bottom bars* outside the box indicate the maximum and minimum extreme precipitation indices projected by the 17 CMIP5 models, respectively. The *upper* and *bottom edges* of the box indicate the range of one standard deviation; the *middle bar* in the box represents the median value, and the *star* in the box represents the MME result

5 Conclusion and discussion

In this study, the simulation capabilities of 17 CMIP5 global climate models and their ensemble were investigated relative to an observed gridded daily dataset CN05.1. Four extreme precipitation indices were adopted to evaluate and project the spatiotemporal features of extreme heavy precipitation events. The results show that these models and the MME can readily capture observed spatial features of precipitation extremes in China

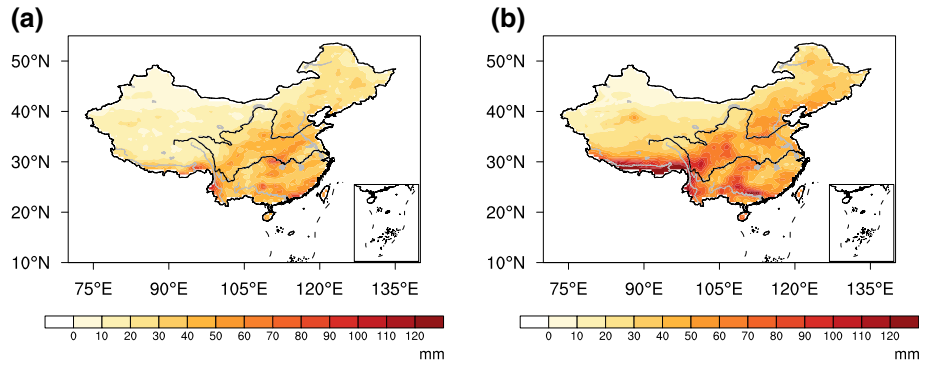

Fig. 12 Spatial distribution of the intermodel standard deviation of changes in R95p projected by the 17 CMIP5 models for the **a** 1.5 °C and **b** 3.5 °C warming targets under the RCP8.5 scenario (unit: mm)

while they are limited in their ability to reproduce temporal features, which is consistent with the results presented by Xu and Xu (2012). This indicates that the ability of these CMIP5 models to simulate the temporal features of extreme precipitation has not obviously improved. Second, as the global mean temperature rise increases from the 1.5 to 5.0 °C warming target, extreme precipitation events in China will become more frequent and more intense. The nationally averaged R25, R50, R95p, and R99p values will increase by 0.26 days/year (8.14 %), 0.11 days/year (25.81 %), 30.41 mm/year (19.69 %), and 30.51 mm/year (69.14 %) for the 1.5 °C warming target and by 1.14 days/year (37.10 %), 0.40 days/year (95.52 %), 88.34 mm/year (57.23 %), and 71.59 mm/year (162.00 %) for the 4.0 °C warming target, respectively, compared with the baseline period (1971–2000) values. Those subregions that are considerably affected by the EASM and experience heavy precipitation events frequently in the baseline climate (e.g., Southwest China, South China and the Yangtze-Huai River Valley) will suffer from an increased number of extreme precipitation days with greater rainfall, while those subregions where extreme precipitation is currently rare (e.g., Northwest China) will experience a relatively minor increase in precipitation extremes; this is consistent with previous research (Zhang et al. 2006; Jiang et al. 2012; Xu et al. 2015).

Admittedly, the models' ability to simulate extreme precipitation indices is lower than their ability to simulate extreme temperature indices (Jiang et al. 2012). The model simulation results show that there is a large dry bias in Southeast China while there is a wet bias in Northwest and North China. The system bias within GCMs and their ability to simulate the features of extreme precipitation is closely related to the ability of the models to simulate atmospheric circulation, such as the Northwest Pacific subtropical high (NPSH) and southwesterly winds (Rajendran et al. 2004; Jiang et al. 2015). Moreover, the simulation bias between GCMs and observation is also attributed to the coarse resolution of global climate models. Regional climate models (RCMs) have finer resolutions and thus are better able to capture the characteristics of climate extremes on a regional scale. Gao et al. (2008) found that the regional climate model RegCM3, which is driven by a GCM, better reproduces the features of precipitation extremes in China because it can capture more detailed geographical features and large-scale precipitation patterns than the underlying GCMs. Additionally, the RCM can effectively remove the false strong precipitation center simulated by the GCM along the southeastern edge of the Tibetan Plateau. Similarly, RCMs with finer resolutions have been increasingly adopted to project the

variations in future extreme precipitation in China (Zhang et al. 2006; Gao et al. 2008; Li and Luo 2011; Gao et al. 2013). Xu et al. (2015) show that the range of uncertainty in projected extreme climate variation in the eight subregions is much greater than that across China as a whole. Thus, the RCMs are urgently needed to better project changes in extreme precipitation at smaller regional scales in China.

In terms of projection results, in this study, the period 1861–1880 was selected to represent the pre-industrial period. Because no instrumental data on global temperatures exist prior to 1850, setting a different pre-industrial time period is scientifically supported (Knutti et al. 2016). To determine the influence of the chosen pre-industrial period on the projected timeframe, we selected three different pre-industrial time periods [1871–1880 (total 10 years), 1861–1890 (total 30 years), and 1861–1900 (total 40 years)] and calculated the median years for eight warming targets. The results show that the projected median year for any specific warming target under the RCP8.5 scenario varies little (range from 1 to 3 years) based on the three selected pre-industrial timeframes. For instance, as the global mean temperature rise increases to 2 °C relative to the pre-industrial timeframe 1861–1880, 1861–1890, 1871–1890, and 1861–1900, the projected median years for the warming target are 2038, 2037, 2037, and 2037, respectively.

The variations in precipitation extremes in China are known to differ based on the models and precipitation indices used. However, in general, the increase in precipitation extremes in China by the end of the twenty-first century is unquestionable (Luo et al. 2005; Feng et al. 2011; Xu et al. 2015). Admittedly, the intermodel uncertainties of the projected precipitation extremes are still large, especially in those regions where the EASM prevails more, as presented in Sect. 4.6. To a large extent, these uncertainties are related to complicated mechanisms responsible for the variation in extreme precipitation across China, including atmospheric circulation anomalies (Gong and Ho 2002; Wang and Li 2005; Ding et al. 2008; You et al. 2011), global warming (Li et al. 2011; Zhao et al. 2010), urbanization (Zhang et al. 2009; Miao et al. 2011), aerosols (Zhao et al. 2006), sea surface temperature (Gong and Ho 2002; Zhou et al. 2008), land-use change (Gao et al. 2003, 2007), geographical features such as the Tibetan Plateau (Wang et al. 2008) at the regional scale, and so on. The atmospheric circulation is undoubtedly one of the most crucial causes of climate extremes. Changes in large-scale circulation, especially the EASM system, are strongly associated with variations in extreme precipitation across China, especially in those regions where the EASM predominates (Zhai et al. 2005; You et al. 2011). After the 1970s (1983–2003), the weaker EASM triggered a change in extreme precipitation in Eastern and Northern China as a result of its inability to penetrate into those region (Xu et al. 2006). Based on the NCEP/NCAR reanalysis data, the strengthening anticyclonic circulation across the Eurasian continent from 1961 to 2003 has facilitated changes in climate extremes in China (You et al. 2011). In the context of global warming, the EASM circulation patterns will strengthen and the unstable local atmospheric stratification will increase, contributing to an increase in precipitation extremes in China by the end of the twenty-first century (Chen 2013). Another large-scale circulation system, the Northwest Pacific subtropical high (NPSH), which is much stronger during the boreal summer, will significantly impact climate change in China during this period. To examine the possible effects of the NPSH on variations in summer heavy rainfall events in China, the temporal correlation coefficients between the extreme precipitation indices and the NPSH indices were calculated for the summer season (June–August) from 1961 to 2005. This revealed that the precipitation extremes in the Yangtze-Huai River Valley correlated most closely with the intensity and position of the NPSH. Taking R95p as an example, the temporal correlation coefficients between the area, intensity, ridge line, and

west-extending ridge point indices of the NPSH and R95p are 0.40, 0.38, −0.29, and −0.26, respectively, all of which exceed the 90 % significant level. This indicates that the intensification, southward and westward movements of the NPSH facilitate the strengthening of precipitation extremes in this subregion. According to the circulation analysis, it is further understood that when the NPSH is stronger and its ridge point is located at 120°E, the southwestern flow along the west segment of the NPSH can transport more moisture to the Yangtze-Huai River Valley, which further promotes the occurrence of heavy rainfall events in this region. That said, other factors (e.g., sea surface temperature, land use) should be explored to elucidate the ocean–atmosphere and land–atmosphere feedback mechanisms affecting the occurrence of precipitation extremes in these subregions.

The above analysis of the possible effects of the NPSH atmospheric circulation system on the interannual variation of precipitation extremes is only based on the observation dataset; however, additional research is necessary to investigate the relationship between the precipitation extremes and possible causes in China utilizing model outputs. In addition, research into whether the above correlation would still be significant in the future climate, as was observed in the historical climate, is needed and will help to elucidate the mechanisms of precipitation extremes and further improve the models' ability to simulate and project this extreme in China.

Acknowledgments We acknowledge the World Climate Research Programme's Working Group on Coupled Modeling, which is responsible for CMIP, and we also thank the climate modeling groups for producing and making their model outputs available. We acknowledge the National Climate Center of the China Meteorological Administration, which provided the observed gridded daily dataset CN05.1 and assisted in the evaluation of these models' simulation capabilities. This research was further jointly supported by the following three projects: the China Meteorological Administration Special Public Welfare Research Fund (Grant No: GYHY201306019), the China Meteorological Administration Climate Change Special Fund (Grant No: CCSF201319), and the Chinese Clean Development Mechanism (Grant No: No. 2013081).

References

Aguilar E, Barry AA, Brunet M, Ekang L et al (2009) Changes in temperature and precipitation extremes in western central Africa, Guinea Conakry, and Zimbabwe, 1955–2006. J Geophys Res 114(D2):356–360

Chen HP (2013) Projected change in extreme rainfall events in China by the end of the 21st century using CMIP5 models. Chin Sci Bull 58(12):1462–1472

Coumou D, Rahmstorf S (2012) A decade of weather extremes. Nat Clim Change 2(7):491–496. doi:10.1038/nclimate1452

Ding Y, Wang Z, Sun Y (2008) Inter-decadal variation of the summer precipitation in East China and its association with decreasing Asian summer monsoon. Part I: observed evidences. Int J Climatol 28(9):1139–1161

Domroes M, Peng G (1988) Climate of China. Springer, Berlin

Feng L, Zhou TJ, Wu B, Li T, Luo JJ (2011) Projection of future precipitation change over China with a high-resolution global atmospheric model. Adv Atmos Sci 28(2):464–476

Field CB, Barros V, Stocker TF, Qing DH et al (2012) Managing the risks of extreme events and disasters to advance climate change adaptation: special report of the intergovernmental panel on climate change, Cambridge University Press, Cambridge

Gao XJ, Luo Y, Lin WT, Zhao ZC, Giorgi F (2003) Simulation of effects of land use change on climate in China by a regional climate model. Adv Atmos Sci 20(4):583–592

Gao XJ, Zhang DF, Chen ZX, Pal JS, Giorgi F (2007) Land use effects on climate in China as simulated by a regional climate model. Sci China Ser D 50(4):620–628
Gao X, Shi Y, Song R, Giorgi F, Wang Y et al (2008) Reduction of future monsoon precipitation over China: comparison between a high resolution RCM simulation and the driving GCM. Meteorol Atmos Phys 100(1–4):73–86
Gao XJ, Wang ML, Giorgi F (2013) Climate change over China in the 21st century as simulated by BCC_CSM1. 1-RegCM4. 0. Atmos Ocean Sci Lett 6(5):381–386
Gong DY, Ho CH (2002) Shift in the summer rainfall over the Yangtze River valley in the late 1970s. Geophys Res Lett. doi:10.1029/2006GL027229
Guo XJ, Huang JB, Luo Y, Zhao ZC, Xu Y (2016) Projection of heat waves over China for eight different global warming targets using 12 CMIP5 models. Theor Appl Climatol. doi:10.1007/s00704-015-1718-1
Haerter JO, Berg P (2009) Unexpected rise in extreme precipitation caused by a shift in rain type? Nat Geosci 2:372–373
Huang J, Sun S, Zhang J (2013) Detection of trends in precipitation during 1960–2008 in Jiangxi province, southeast China. Theor Appl Climatol 114(1–2):237–251
IPCC (2007) Climate change 2007: the physical science basis. In: Solomon S, Qin D, Manning M, Chen Z, Marquis M, Averyt KB, Tignor M, Miller HL (eds) Contribution of working group I to the fourth assessment report of the intergovernmental panel on climate change. Cambridge University Press, Cambridge
IPCC (2013) Climate change 2013: the physical science basis. In: Stocker TF, Qin D, Plattner G-K, Tignor M, Allen SK, Boschung J, Nauels A, Xia Y, Bex V, Midgley PM (eds) Contribution of working group I to the fifth assessment report of the intergovernmental panel on climate change. Cambridge University Press, Cambridge
Ji ZM, Kang SC (2015) Evaluation of extreme climate events using a regional climate model for China. Int J Climatol 35(6):888–902
Jiang DB, Fu YH (2012) Climate change over China with a 2 °C global warming. Chin J Atmos Sci 36(2):234–246
Jiang Z, Song J, Li L, Chen W, Wang Z, Wang J (2012) Extreme climate events in China: IPCC-AR4 model evaluation and projection. Clim Change 110:385–401
Jiang ZH, Li W, Xu JJ, Li L (2015) Extreme precipitation indices over China in CMIP5 models. Part I: model evaluation. J Clim 28(21):8603–8619
Kanitkar T (2015) What should the climate goal be, 1.5 °C or 2 °C? Journal 5(2):60–72
Klein Tank AMG, Peterson TC, Quadir DA, Dorji S, Zou X et al (2006) Changes in daily temperature and precipitation extremes in central and south Asia. J Geophys Res. doi:10.1029/2005JD006316
Knutti R, Rogelj J, Sedláček J, Fischer EM (2016) A scientific critique of the two-degree climate change target. Nat Geosci 9(1):13–18
Lang XM, Sui Y (2013) Changes in mean and extreme climates over China with a 2 °C global warming. Chin Sci Bull 58(12):1453–1461
Li T, Luo JJ (2011) Projection of future precipitation change over China with a high-resolution global atmospheric model. Adv Atmos Sci 28(2):464–476
Li B, Zhou TJ (2010) Projected climate change over China under SRES A1B scenario: multi-model ensemble and uncertainties. Adv Atmos Sci 6:270–276
Li HM, Feng L, Zhou TJ (2011) Multi-model projection of July–August climate extreme changes over China under CO_2 doubling. Part I: precipitation. Adv Atmos Sci 28:433–447. doi:10.1007/s00376-010-0013-4
Luo Y, Zhao ZC, Xu Y, Gao XJ, Ding YH (2005) Projections of Climate Change over China for the 21st century. Acta Meteorol Sin 19(4):401
Meehl GA, Hu A, Tebaldi C, Arblaster JM, Washington WM et al (2012) Relative outcomes of climate change mitigation related to global temperature versus sea-level rise. Nat Clim Change 2(8):576–580
Miao S, Chen F, Li Q, Fan S (2011) Impacts of urban processes and urbanization on summer precipitation: a case study of heavy rainfall in Beijing on 1 August 2006. J Appl Meteorol Clim 50(4):806–825
O'Gorman PA, Schneider T (2009) The physical basis for increases in precipitation extremes in simulations of 21st-century climate change. Proc Natl Acad Sci 106(35):14773–14777. doi:10.1073/pnas.0907610106
Qian WH, Lin X (2005) Regional trends in recent precipitation indices in China. Meteorol Atmos Phys 90(3–4):193–207. doi:10.1007/s00703-004-0101-z
Rajendran K, Kitoh A, Yukimoto S (2004) South and East Asian summer monsoon climate and variation in the MRI coupled model (MRI-CGCM2). J Climate 17(4):763–782
Sun Y, Solomon S, Dai A, Portmann RW (2007) How often will it rain? J Clim 20(19):4801–4818

Trenberth KE, Dai AG, Rasmussen RM, Parsons DB (2003) The changing character of precipitation. Bull Am Meteorol Soc 84(9):1205–1217
Tschackert P (2015) 1.5 °C or 2 °C: a conduit's view from the science-policy interface at COP20 in Lima, Peru. Clim Change Resp 2:1–11. doi:10.1186/s40665-015-0010-z
UNFCCC (United Nations Framework Convention on Climate Change) (2009) Decision 2/CP.15 Copenhagen Accord: 4–10. http://unfccc.int/resource/docs/2009/cop15/eng/l07.pdf
UNFCCC (United Nations Framework Convention on Climate Change) (2013) National inventory submissions 2013. United Nations Framework Convention on Climate Change (UNFCCC). Bonn, Germany. http://unfccc.int/national_reports/annex_i_ghg_inventories/national_inventories_submissions/items/7383.php
Wang YQ, Li Z (2005) Observed trends in extreme precipitation events in China during 1961–2001 and the associated changes in large-scale circulation. Geophys Res Lett. doi:10.1029/2005GL022574
Wang B, Bao Q, Hoskins B, Wu G, Liu Y (2008) Tibetan Plateau warming and precipitation changes in East Asia. Geophys Res Lett. doi:10.1029/2008GL034330
Wang K, Wang L, Wei YM, Ye M (2013) Beijing storm of July 21, 2012: observations and reflections. Nat Hazards 67(2):969. doi:10.1007/s11069-013-0601-6
Westra S, Alexander LV, Zwiers FW (2013) Global increasing trends in annual maximum daily precipitation. J Climate 26(11):3904–3918
World Meteorological Organization Current Extreme Weather Events (WMO) (2010). www.wmo.int/pages/mediacentre/news/extremeweathersequence_en.html
Wu J, Gao XJ (2013) A gridded daily observation dataset over China region and comparison with other datasets. Chin J Geophys 56(4):1102–1111
Xu Y, Xu CH (2012) Preliminary assessment of simulations of climate changes over China by CMIP5 multimodels. Atmos Oceanic Sci Lett 5(6):489–494
Xu M, Chang CP, Fu C, Qi Y, Robock A et al (2006) Steady decline of east Asian monsoon winds, 1969–2000: evidence from direct ground measurements of wind speed. J Geophys Res 111:D24111. doi:10.1029/2006JD007337
Xu Y, Wu J, Shi Y, Zhou BT, Li RK, Wu J (2015) Change in extreme climate events over China based on CMIP5. Atmos Oceanic Sci Lett 8(4):185–192
Yin H, Li C (2001) Human impact on floods and flood disasters on the Yangtze River. Geomorphology 41(2):105–109
You QL, Kang SC, Aguilar E, Pepin N, Flügel WA et al (2011) Changes in daily climate extremes in China and their connection to the large scale atmospheric circulation during 1961–2003. Clim Dyn 36(11–12):2399–2417
Zhai PM, Zhang XB, Wan H, Pan XH (2005) Trends in total precipitation and frequency of daily precipitation extremes over China. J Clim 18(7):1096–1108
Zhang Y, Xu Y, Dong W, Cao L, Sparrow M (2006) A future climate scenario of regional changes in extreme climate events over China using the PRECIS climate model. Geophys Res Lett. doi:10.1029/2006GL027229
Zhang CL, Chen F, Miao SG, Li QC, Xia XA et al (2009) Impacts of urban expansion and future green planting on summer precipitation in the Beijing metropolitan area. J Geophys Res. doi:10.1029/2008JD010328
Zhang L, Ding YH, Wu TW, Xin XG, Zhang YW et al (2013a) The 21st century annual mean surface air temperature change and 2 °C warming threshold over the globe and China as projected by the CMIP5 models. Acta Meteorol Sin 71(6):1047–1060
Zhang DL, Lin YH, Zhao P, Yu XD, Wang SQ et al (2013b) The Beijing extreme rainfall of 21 July 2012:"Right results" but for wrong reasons. Geophys Res Lett 40(7):1426–1431
Zhao C, Tie X, Lin Y (2006) A possible positive feedback of reduction of precipitation and increase in aerosols over eastern central China. Geophys Res Lett. doi:10.1029/2006GL025959
Zhao P, Yang S, Yu RC (2010) Long-term changes in rainfall over eastern China and large-scale atmospheric circulation associated with recent global warming. J Clim 23(6):1544–1562
Zhou T, Yu R, Li H, Wang B (2008) Ocean forcing to changes in global monsoon precipitation over the recent half-century. J Clim 21(15):3833–3852
Zhou BT, Han Wen QZ, Xu Y, Song LC, Zhang XB (2014) Projected changes in temperature and precipitation extremes in China by the CMIP5 multimodel ensembles. J Clim 27:6591–6611
Zong Y, Chen X (2000) The 1998 flood on the Yangtze, China. Nat Hazards 22(2):165–184